

## Article

# A Novel Spinel Ferrite-Hexagonal Ferrite Composite for Enhanced Magneto-Electric Coupling in a Bilayer with PZT

Sujoy Saha <sup>1</sup>, Sabita Acharya <sup>1</sup>, Maksym Popov <sup>1,2</sup>, Theodore Sauyet <sup>3</sup>, Jacob Pfund <sup>3</sup>, Rao Bidthanapally <sup>1</sup>, Menka Jain <sup>3</sup>, Michael R. Page <sup>4</sup> and Gopalan Srinivasan <sup>1,\*</sup>

<sup>1</sup> Department of Physics, Oakland University, Rochester, MI 48309, USA; sujoysaha@oakland.edu (S.S.); sabitaacharya@oakland.edu (S.A.); maxim\_popov@univ.kiev.ua (M.P.); burao@oakland.edu (R.B.)

<sup>2</sup> Institute of High Technologies, Taras Shevchenko National University of Kyiv, 01601 Kyiv, Ukraine

<sup>3</sup> Department of Physics, University of Connecticut, Storrs, CT 06269, USA; theodore.sauyet@uconn.edu (T.S.); jacob.pfund@uconn.edu (J.P.); menka.jain@uconn.edu (M.J.)

<sup>4</sup> Materials and Manufacturing Directorate, Air Force Research Laboratory, Wright-Patterson Air Force Base, Dayton, OH 45433, USA; michael.page.16@us.af.mil

\* Correspondence: srinivas@oakland.edu

**Abstract:** The magnetoelectric effect (ME) is an important strain mediated-phenomenon in a ferromagnetic-piezoelectric composite for a variety of sensors and signal processing devices. A bias magnetic field, in general, is essential to realize a strong ME coupling in most composites. Magnetic phases with (i) high magnetostriction for strong piezomagnetic coupling and (ii) large anisotropy field that acts as a built-in bias field are preferred so that miniature, ME composite-based devices can operate without the need for an external magnetic field. We are able to realize such a magnetic phase with a composite of (i) barium hexaferrite (BaM) with high magnetocrystalline anisotropy field and (ii) nickel ferrite (NFO) with high magnetostriction. The BN<sub>x</sub> composites, with (100 – x) wt.% of BaM and x wt.% NFO, for x = 0–100, were prepared. X-ray diffraction analysis shows that the composites did not contain any impurity phases. Scanning electron microscopy images revealed that, with an increase in NFO content, hexagonal BaM grains become prominent, leading to a large anisotropy field. The room temperature saturation magnetization showed a general increase with increasing BaM content in the composites. NFO rich composites with x ≥ 60 were found to have a large magnetostriction value of around –23 ppm, comparable to pure NFO. The anisotropy field H<sub>A</sub> of the composites, determined from magnetization and ferromagnetic resonance (FMR) measurements, increased with increasing NFO content and reached a maximum of 7.77 kOe for x = 75. The BN<sub>x</sub> composite was cut into rectangular platelets and bonded with PZT to form the bilayers. ME voltage coefficient (MEVC) measurements at low frequencies and at mechanical resonance showed strong coupling at zero bias for samples with x ≥ 33. This large in-plane H<sub>A</sub> acted as a built-in field for strong ME effects under zero external bias in the bilayers. The highest zero-bias MEVC of ~22 mV/cm Oe was obtained for BN75-PZT bilayers wherein BN75 also has the highest H<sub>A</sub>. The Bilayer of BN95-PZT showed a maximum MEVC ~992 mV/cm Oe at electromechanical resonance at 59 kHz. The use of hexaferrite–spinel ferrite composite to achieve strong zero-bias ME coupling in bilayers with PZT is significant for applications related to energy harvesting, sensors, and high frequency devices.

**Keywords:** magnetoelectric; spinel ferrite; hexagonal ferrite; ferroelectric; composite



**Citation:** Saha, S.; Acharya, S.; Popov, M.; Sauyet, T.; Pfund, J.; Bidthanapally, R.; Jain, M.; Page, M.R.; Srinivasan, G. A Novel Spinel Ferrite-Hexagonal Ferrite Composite for Enhanced Magneto-Electric Coupling in a Bilayer with PZT. *Sensors* **2023**, *23*, 9815. <https://doi.org/10.3390/s23249815>

Academic Editor: Arcady Zhukov

Received: 17 October 2023

Revised: 6 December 2023

Accepted: 11 December 2023

Published: 14 December 2023



**Copyright:** © 2023 by the authors. Licensee MDPI, Basel, Switzerland. This article is an open access article distributed under the terms and conditions of the Creative Commons Attribution (CC BY) license (<https://creativecommons.org/licenses/by/4.0/>).

## 1. Introduction

Multiferroic materials exhibit more than one ferroic order, such as ferromagnetism, ferroelectricity, and ferroelasticity [1]. They have recently attracted significant attention due to their potential for applications in spintronics, magneto-electrics, nonvolatile memories, sensors, and electrically tunable magnetic microwave devices [2,3]. A ferromagnetic–ferroelectric composite is a multiferroic that shows a variation of its ferroelectric order parameters when subjected to an external magnetic field, direct magnetoelectric (ME) effect, or changes in magnetic parameters in an applied electric field, converse ME effect [4]. In

ME materials, the induced electric polarization  $P$  is related to the applied external magnetic field  $H$  by  $P = \alpha H$ , where  $\alpha$  is a second order ME-susceptibility tensor. Another parameter of importance is the ME voltage coefficient (MEVC)  $\alpha_E = \delta E / \delta H$ , where  $\delta E$  is the induced electric field due to applied magnetic field  $\delta H$ , and is related to  $\alpha$  by  $\alpha = \epsilon_0 \epsilon_r \alpha_E$ , where  $\epsilon_r$  is the relative permittivity of the material. According to models for the ME effects in single-phase materials, the upper bound  $\alpha$  is limited to the relation  $\alpha \leq (\mu \epsilon)^{1/2}$ , where  $\mu$  and  $\epsilon$  are the permeability and permittivity of the material, respectively [5]. One known single-phase multiferroic with a large  $\alpha$  at room temperature is BiFeO<sub>3</sub> [6]. In composite ME materials,  $\alpha$  can be enhanced by exploiting the strain mediated interactions between the two phases [4].

To obtain the maximum ME voltage coefficient ( $\alpha_E$ ) in a ferromagnetic–ferroelectric composite, an optimized magnitude of the DC magnetic bias field  $H$  is needed. A maximum in the  $\alpha_E$  occurs when the piezomagnetic coefficient  $q = d\lambda/dH$  (where  $\lambda$  is the magnetostriction) of ferro/ferrimagnetic component of the composite is also maximum. Hence, a bias magnetic field is generally essential to achieve a strong ME response. The need for a bias field, however, could be eliminated with a self-bias in the ferromagnetic. There are several avenues to accomplish the self-bias condition, such as a large magneto-crystalline anisotropy field or the use of a functionally graded ferromagnet [7–9]. Other avenues include the use of a compositionally graded ferromagnetic phase [10]. There are several experimental findings [11–13] and theoretical models [11–13] on graded ME composites. In laminated composites, changing the mechanical resonance modes through electrical connectivity evokes zero bias coupling when the bending strain activates a built-in bias [9]. Thin films that rely on magnetic field dependence of resonant frequency and angular dependence of exchange bias field [14,15] can also show a zero-bias ME effect. It is also shown that a homogeneous magnetostrictive phase can also produce a zero bias ME effect [16]. Cofired layered composites consisting of textured Pb(Mg<sub>1/3</sub>Nb<sub>2/3</sub>)O<sub>3</sub>-PbTiO<sub>3</sub> (PMN-PT) and Cu and Zn doped NiFe<sub>2</sub>O<sub>4</sub> show a giant zero-bias ME coefficient  $\sim 1000$  mV/cm Oe [17], wherein built in stress induces zero-bias effect. Very recently, Huang et. al. [18] have shown a very large self-bias ME effect with LiNbO<sub>3</sub> single crystal and Ni trilayers with residual stress engineering by using Ni as the electrode and the piezomagnetic layer simultaneously using RF sputtering. Wu et. al. [19] have shown that large sensitivity in PMN-PT-Metglass ME sensors by utilizing shear stress induced self-bias effect. Annapureddy et. al. [20] have obtained a large self-bias effect ( $\sim 4200$  mV/cm Oe) by utilizing the graded magnetization. To date, all the reported self-bias effects are sample specific. The role of the sample configuration and/or preparation is crucial to obtain the self-bias.

This work focuses on a novel, never-before-used approach for a self-biased ME composite with the use of a ferromagnetic layer consisting of both M-type barium ferrite hexagonal ferrite, BaO 6Fe<sub>2</sub>O<sub>3</sub> (BaM), with uniaxial anisotropy on the order of  $\sim 17.4$  kOe, and nickel ferrite NiFe<sub>2</sub>O<sub>4</sub> with high magnetostriction and piezomagnetic coefficient  $q$  [21]. Composites of BaM-NFO with (100 –  $x$ ) wt.% of BaM and  $x$  wt.% of NFO, (BN $x$ ), were prepared by sintering powders of both ferrites. X-ray diffraction revealed the presence of both BaM and NFO and the absence of impurity phases. Scanning electron microscopy images showed crystallites of both ferrites. Magnetization measurements at room temperature for static fields up to 2 T showed an increase in  $4\pi M$  with increasing BaM content in the composite. Magnetostriction  $\lambda$  measurements for BN $x$  indicated an increase with increasing  $x$ , and for  $x > 65$ , reached values comparable that of pure NFO. High frequency measurements were carried out to determine the anisotropy field  $H_A$  from dependence of the ferromagnetic resonance (FMR) frequency  $f_r$  on static magnetic field  $H$ . The in-plane  $H_A$  values in BN $x$  were found to be well above the value of 500 Oe for pure NFO. These composites show a large piezomagnetic coefficient and large magnetocrystalline anisotropy simultaneously, which is somewhat unique to this spinel ferrite–hexaferrite composite. Platelets of sintered BN $x$  were bonded to PZT to form bilayers for ME voltage coefficient (MEVC) measurements that showed a significant zero-field ME effects. Details on results of the studies are provided in the following sections.

## 2. Experiment

### 2.1. Materials

The ferrite composites were prepared by the traditional ceramic synthesis techniques. Micrometer-sized polycrystalline NFO and BaM powders were first synthesized separately. High purity NiO, BaCO<sub>3</sub>, and Fe<sub>2</sub>O<sub>3</sub> were mixed and ball milled for 8 h. The powders were dried and pre-sintered at 900 °C for 6 h. The pre-sintered powders were ball milled again, and then sintered at 1200 °C for 6 h. Composites of (100 – x) wt.% BaM-x wt% NFO (BN<sub>x</sub>) (x = 5, 9, 13, 33, 38, 41, 44, 47, 60, 75, 85 and 95) were prepared by mixing the ferrite powders. A binder, 2% PVA, was added to the powder and pressed into disks (diameter ~18 mm and thickness ~2 mm) by applying uniaxial pressure of 250 MPa. The disks of BN<sub>x</sub> were finally sintered at 1250 °C for 6 h.

### 2.2. Characterizations

The crystal structure of the composites was characterized by a powder X-ray diffractometer (Miniflex, Rigaku, Japan) at room temperature. Morphological features of the samples were studied with an SEM (JSM-6510/GS, JEOL, Tokyo, Japan). Magnetostriction of the composite on rectangular platelets was measured using a strain gauge and a strain indicator/recorder (P3, Micro-Measurements, Wendell, NC, USA). The magnetic field was applied parallel to the sample plane and along the length (direction-1) of the gauge, and magnetostriction measured in this configuration is labeled  $\lambda_{11}$ . Magnetization at room temperature as a function of H was measured with an Evercool Physical Property Measurement System (PPMS, Quantum Design Inc., San Diego, CA, USA). Ferromagnetic resonance (FMR) measurements were conducted on thin rectangular platelets of the composites with the sample placed on a coplanar waveguide and with the magnetic field H parallel to the sample plane and along its length. A vector network analyzer (E8361A, Agilent, Santa Clara, CA, USA) was used to record profiles of the scattering matrix  $S_{21}$  vs. frequency f for a series of H. Measurements of ME coupling strengths were completed on a bilayer of BN<sub>x</sub> and vendor-supplied PZT that was bonded with a thin layer of epoxy. Composite platelets of dimensions 10 mm × 5 mm and 1 to 1.5 mm in thickness, and 0.3 mm thick PZT plates of similar lateral dimensions as the composite, were used. The ME voltage coefficient (MEVC) measurements were completed by subjecting the bilayer to an ac magnetic field  $H_{ac}$  and a bias field H. Both H- and f-dependence of the MEVC were measured for both the magnetic fields parallel each other and either parallel or perpendicular to the sample plane.

## 3. Results

### 3.1. Structural Characterization

Representative powder X-ray diffraction (XRD) patterns for the BN<sub>x</sub> samples are shown in Figure 1. XRD patterns of other BN<sub>x</sub> compositions are shown in the Figure S1 in the Supplementary Materials. The XRD patterns show diffraction peaks from NFO and BaM. With increasing x-values, the NFO lines become stronger and BaM lines get weaker, as expected. This is due to the reduced weight fraction of the BaM phase as we increase x. X-ray intensity corresponding to a particular phase is proportional to the weight fraction of the phase. We have deliberately varied the weight fraction of the NFO/BaM phases, and when the NFO weight fraction is increased, the line intensity corresponding to NFO becomes stronger; likewise, BaM intensity gets weaker. A small amount of an impurity phase, identified as antiferromagnetic Ba<sub>5</sub>Fe<sub>2</sub>O<sub>8</sub>, is present only in BN<sub>41</sub>, BN<sub>44</sub>, and BN<sub>75</sub> [22]. Usually, Ba<sub>5</sub>Fe<sub>2</sub>O<sub>8</sub> type impurities (5BaO + Fe<sub>2</sub>O<sub>3</sub>) occur during the sintering of BaO and Fe<sub>2</sub>O<sub>3</sub> based ferrites, especially in BaFe<sub>12</sub>O<sub>19</sub> [22]. However, since Ba<sub>5</sub>Fe<sub>2</sub>O<sub>8</sub> is antiferromagnetic, the overall ME character of the BN<sub>x</sub>-PZT bilayers is expected to be unaffected.

Representative SEM images for BN<sub>x</sub> (x = 5, 33, 60 and 95) are shown in Figure 2. The gradual increase in the grain size in the BN composites with increasing x (also in Supplementary Figure S2) may indicate that NFO aids in the growth of hexagonal BaM grains for x ≥ 9. Large grains are absent in BN<sub>5</sub>, but a closer examination of the surface

morphology shows hexagonal-like features with grain size less than 2  $\mu\text{m}$ . With increasing NFO content, grains larger than 5  $\mu\text{m}$  are present. For  $x > 41$ , the number of large grains reduces again. For the highest content of NFO (BN95), we observe a similar grain distribution as pure NFO (Supplementary Figure S2). BN5 also shows a similar grain distribution as pure BaM. When the weight fraction of the BaM phase is high ( $x \sim 5$ ), the composite is more likely to behave as pure BaM. Hence, the corresponding morphological features of composites with high BaM content should also look like pure BaM. Similarly, when the weight fraction ( $x > 41$ ) of NFO is increased, the composites tend to show a reduction in BaM grains. Barium ferrite itself tends to form hexagonal grains [23] and, with a tweak in the synthesis process, the particle shape can be made nearly spherical [24]. In our case, the processing has a large impact on the grain growth on these composites. The stabilization of the typical hexagonal BaM grains amongst NFO particles is worth noting.

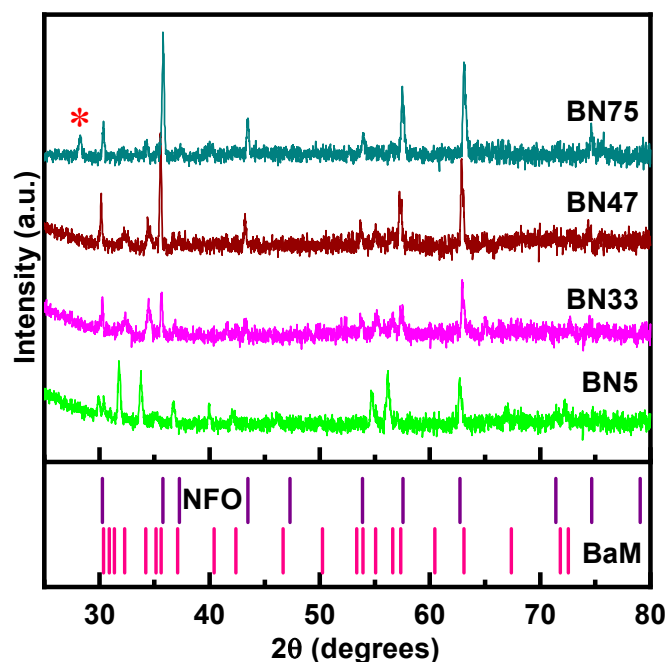


**Figure 1.** Representative X-ray diffraction data for BN $x$  composites. All the composites bear the signatures of NFO and BaM. The stick patterns for NFO and BaM are shown in the bottom pane to visualize the one-to-one correspondence of the Bragg positions of each phase to the respective NFO and BaM lines. BN75 contains a small amount of an impurity phase,  $\text{Ba}_5\text{Fe}_2\text{O}_8$ , and is denoted by a star.

The XRD results in Figure 1 and the SEM images of Figure 2 are indicators of the absence of any significant amount of impurity phases of crystal structures apart from spinel and hexagonal phases. An in-depth investigation and analysis of the crystal and magnetic structures are in order. For example, possible migration of Ni-ion from the spinel phase to the hexagonal phase has to be addressed since the M-type hexagonal phase also has the spinel blocks. Such an investigation, however, is not the primary focus of this particular study.

### 3.2. Magnetic Characterization

We have carried out room-temperature measurements of the magnetization,  $4\pi\text{M}$ , of the composites as a function of applied magnetic field  $H$ . Representative  $4\pi\text{M}$  vs.  $H$  data are shown in Figure 3 and Figure S3. The  $M$  vs.  $H$  loops show hysteresis and remanence as expected, and the saturation values of  $M$  increases with increasing BaM contents in the composites. The  $H$ -values for saturation of the magnetization is less than 3 kOe for NFO rich composites, and it increase as the amount of BaM increases. The magnetization  $4\pi\text{M}$

at  $H = 20$  kOe increases from 2.90 kG for BN95 to 4 kG for BN33. The highest value of remanent  $4\pi M$  of 1.04 kG was measured for BN75.

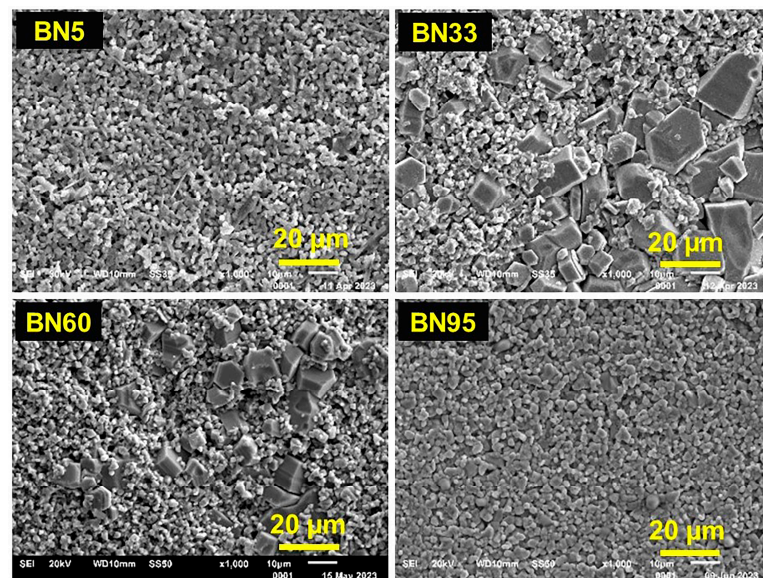


**Figure 2.** SEM images for BN5, BN33, BN60, and BN95 composites. There are no notable features in the image for BN5. Well-defined hexagonal grains corresponding to the BaM phase are seen in BN33 and BN60. BN95 does not show any hexagonal grain.

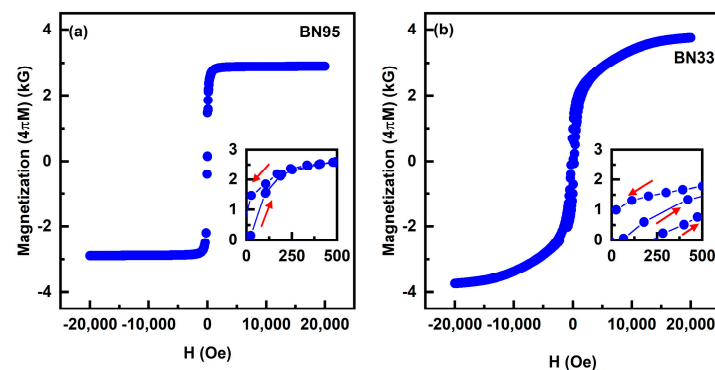


**Figure 3.** Room-temperature magnetization  $4\pi M$  vs. magnetic field  $H$  data for (a) BN95 and (b) BN33 samples. The insets for low  $H$ -values clearly show the expected hysteresis and remanence in the  $M$  vs.  $H$  data. The arrows in the inset indicate which way the magnetic field increases or decreases.

Since the magnetostriction  $\lambda$  is one of the key parameters that determine the strength ME interaction, we measured its value for the BN $x$  composites. The measurements were completed with a strain gauge and a strain indicator and, for  $H$ , was applied parallel to the sample plane and to the length of the strain gauge. Data on the magnetostriction  $\lambda_{11}$  vs.  $H$  are shown in Figure 4. The samples exhibit negative values for  $\lambda_{11}$  as expected since both NFO and BaM have negative  $\lambda_{11}$  values [25,26]. None of the  $\lambda_{11}$  values for the composites in Figure 3 show saturation for the maximum  $H$ -values of  $\sim 3$  kOe. With increases in the NFO content,  $\lambda_{11}$  values at 3 kOe increase and tend to show similar behavior as pure NFO (shown in the inset of Figure 4). The highest value of  $\lambda_{11} \sim -23$  ppm was measured for BN60, and similar values were obtained for  $x \geq 60$ . Our measurements of pure BaM showed  $\lambda_{11} = -1$  ppm at 2.7 kOe. Hence, it is clear that the NFO phase is the major contributor to the net magnetostriction of BN $x$  composites.

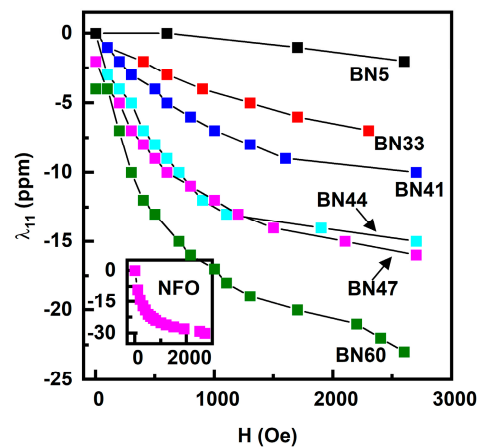


**Figure 4.** Magnetostriction,  $\lambda_{11}$  vs.  $H$  data measured parallel to the in-plane  $H$  for BN $x$  composites. The magnetic field was applied parallel to the length of the sample and the strain gauge.  $\lambda_{11}$  for pure NFO is shown in the inset.

### 3.3. Ferromagnetic Resonance

A key objective of this work is to achieve large enough magneto-crystalline anisotropy field  $H_A$  in BN $x$  to realize a strong zero-bias ME effect in a composite with PZT. The magnetization data in Figure 3 and Figure S3 indicate a large remnant magnetization, as high as 1 kG, which is clear evidence for a large  $H_A$ . We utilized ferromagnetic resonance (FMR) studies in combination with the magnetization data to determine  $H_A$ . Ferrite platelets, rectangular in shape, were placed in an S-shaped coplanar waveguide and excited with microwave power from a VNA. Profiles of the scattering matrix  $S_{21}$  as a function of frequency  $f$  were recorded. Figure 5 shows such profiles for a series of in-plane  $H$  along the sample length. For  $x$  values  $< 10$ , a single resonance mode was seen in the 50 GHz range (See Supplementary Figure S4). As NFO content increased, two resonance modes were seen as in Figure 5, one in the frequency range 3–20 GHz and another in the range 40–60 GHz. The  $S_{21}$  vs.  $f$  profiles in Figure 5 (and Figure S4) show clear asymmetry in the shape of the resonance absorption signals which can be attributed to the variations in the magnitudes of coupling between resonator and the transmission line at frequencies below and above the resonance. Such an asymmetry is not generally observed in cavity-type FMR measurements at a fixed frequency. Also, this effect is negligible for resonance modes with relatively narrow linewidth. However, in the case of transmission line broadband measurement systems and resonances with frequency-width of the order of a few GHz, asymmetry may manifest. Another possible factor is the frequency-dependent background absorption of the coplanar line, which superimposes on absorption through the resonator and leads to significant distortion of the resultant profile. Such asymmetry is most likely to occur at U-band frequencies, where any imperfections of the stripline, connectors, or shielding may unpredictably affect the shape of stripline transmission characteristics. The resonance frequency was estimated from frequency of maximum absorption in the profiles in Figure 5. As discussed, next, the resonance mode at the low frequency region in Figure 5 is due to FMR in NFO whereas the higher frequency resonance is a magneto-dielectric mode in the composite [27].

The  $H$ -dependence of the low- and high frequency mode frequencies  $f_r$  are shown in Figure 6 (and in Supplementary Figure S5). Data on  $f_r$  vs.  $H$  for the low-frequency mode are shown in Figure 6a for BN33 and BN60. With  $f_r$  increasing from 8.6 GHz at  $H = 1$  kOe to 15.9 GHz for  $H = 3.5$  kOe for BN60, which amounts to an increase in  $f_r$  at the rate 2.8 GHz/kOe. A similar rapid increase in  $f_r$  with  $H$  is seen in Figure 6a for BN33. Based on the rate of change in  $f_r$  with  $H$ , one may associate this mode with FMR in NFO. Figure 6b shows  $f_r$  vs.  $H$  for the high frequency mode for BN33 and BN60. In Figure 5 and Figure S5, this mode shows a variation in  $f_r$  with  $H$  that could be approximated to a linear increase  $\sim 1.3$  GHz/kOe. This slow variation in  $f_r$  with  $H$  is indicative of a magneto-dielectric mode

in the composite platelet. This mode is not of importance for the current study and is not considered in further analysis [27].

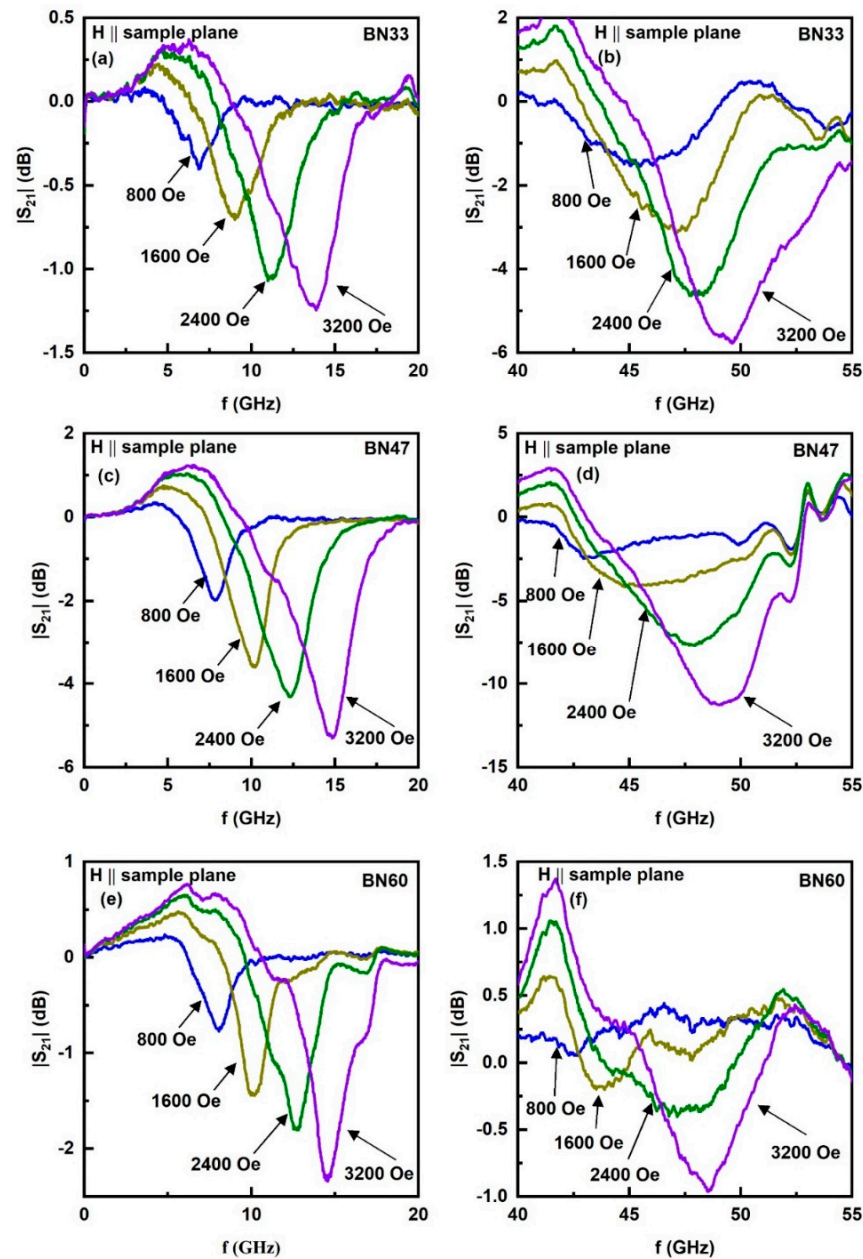


**Figure 5.** Profiles of  $S_{21}$  vs.  $f$  showing resonances in BN33, BN47, and BN60 composites for in-plane static magnetic fields. The absorption in the profiles in (a,c,e) for 5–20 GHz is due to ferromagnetic resonance in the NFO contents of BN $x$ . Profiles in (b,d,f) show absorption due to a magneto-dielectric mode in the composites.

The built-in bias due to magnetic anisotropy field  $H_A$  in the composites is a key parameter that accounts for the zero-bias ME coupling in bilayers of the ferrite composites with PZT, as discussed later. There are several avenues for the determination of  $H_A$ , such as direct measurements and from  $M$  vs.  $H$  data. We utilized FMR results in combination with magnetization values to estimate  $H_A$ . Data on  $f_r$  vs.  $H$  in Figure 7 (and Figure S5) were fitted to appropriate expression for  $f_r$  to determine the effective magnetization  $4\pi M_{\text{eff}} = 4\pi M + H_A$ , where  $4\pi M$  is the magnetization and  $H_A$  is the magnetocrystalline anisotropy field. It is essential to note that  $4\pi M$  is not the saturation magnetization since the  $M$  vs.  $H$  in Figure 3 (and Figure S3) clearly indicate that there is no saturation of  $M$  with

H for several of the composites used in this study. We instead used the average value of  $4\pi M$  for H-values for FMR profiles in Figure 5.

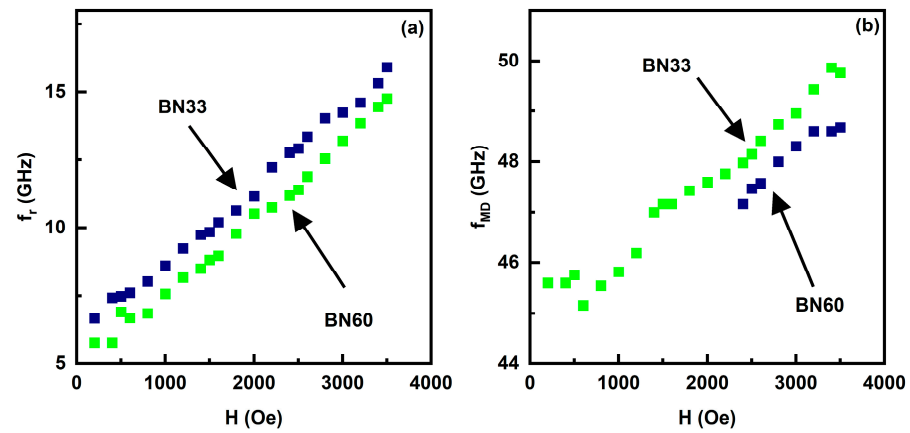


**Figure 6.** Ferromagnetic resonance frequency  $f_r$  as a function of H for (a) FMR observed in the low frequency region in Figure 5 and (b) magneto-dielectric mode frequency vs. H for BN<sub>x</sub> composites.

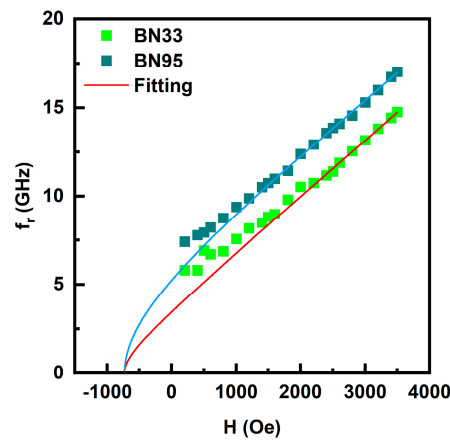


**Figure 7.** Fitting of the FMR data on  $f_r$  vs. H to Equation (1).

The resonance frequency  $f_r$  for FMR mode is given by the Kittel equation,

$$f_r = \gamma \left( \left( H + (N_z - N_x)4\pi M_{eff} \right) \left( H + (N_y - N_x)4\pi M_{eff} \right) \right)^{\frac{1}{2}} \quad (1)$$

where  $\gamma$  is the gyromagnetic ratio, H is the in-plane external magnetic field along the x-direction,  $N_x$ ,  $N_y$ , and  $N_z$  are the demagnetization factors along the length, width, and thickness of the platelet, respectively. These values are shown in Table 1 for each of the composites in which FMR mode was observed. The data in Figure 7 (and Supplementary Figure S5) were fitted to Equation (1) to determine  $4\pi M_{eff}$ . The Kittel equation in the presented form is, strictly speaking, applicable to the ferromagnetic samples of ellipsoidal shape, magnetized to saturation, and has uniform static and dynamic magnetization. However, the samples presented in this investigation had a parallelepiped shape rather than an ellipsoidal one. That means that, even after an external magnetic field  $H > N_x 4\pi M$  was applied and domain structure was suppressed, the sample was still not in a uniformly magnetized state. There were regions of ferrite present (mostly around edges and corners [28]) where the magnetization deviates from the direction of bias magnetic field. Thus, an even larger H should be applied before the magnetic state of the sample becomes uniform and the Kittel equation becomes applicable. For these reasons, we took only the high-frequency (and high-field) portion of the dependencies shown in Figure 7 and fit them with the Kittel equation to obtain the most reliable fitting parameters.

**Table 1.** Demagnetization factors for BN composites.

Sample	Demagnetization Factors		
	$N_x$	$N_y$	$N_z$
BN33	0.11164	0.31851	0.56984
BN38	0.11238	0.32595	0.56167
BN41	0.10642	0.2778	0.61578
BN44	0.10168	0.30318	0.59514
BN47	0.11442	0.2892	0.59638
BN60	0.16197	0.31884	0.51919
BN75	0.19305	0.40187	0.40508
BN85	0.12413	0.22542	0.65045
BN95	0.10323	0.20369	0.69308
NFO	0.11812	0.40771	0.47417

Estimated values of the gyromagnetic ratio  $\gamma$  and  $4\pi M_{\text{eff}}$  from the fits and the average values of  $4\pi M$  for  $H = 1$  kOe to 3.5 kOe (from  $M$  vs.  $H$  data) are given in Table 2. The values of  $\gamma$  range from 3.17 GHz/kOe for  $x = 33$  to 2.61 GHz/kOe for  $x = 0.60$ , which are comparable to the 3.0 to 3.2 GHz/kOe value reported for pure NFO [29,30]. The value of the anisotropy  $H_A$  estimated from FMR data is also given in Table 2, and will have an error of at least 0.5 kOe. The anisotropy field  $H_A$  is positive for  $x = 33$ –95, indicative of in-plane anisotropy for all the polycrystalline BN $x$  composites with  $x = 33$ –95. The anisotropy increases from  $\sim 0.90$  kOe for  $x = 33$  to  $\sim 7.77$  kOe for  $x = 75$ . A further increase in  $x$  results in a decrease in  $H_A$ , but the in-plane character of the anisotropy remains. One may therefore infer from these  $H_A$  -values that a majority of BaM crystallites in  $x = 33$ –95 have a unique in-plane orientation leading to positive values of magnetic anisotropy. With increasing value of NFO content in  $x \geq 33$ , the higher concentration of NFO appears to promote the growth of BaM crystallites with in-plane orientation for the  $c$ -axis and a net in-plane anisotropy field that reaches a maximum value for  $x = 75$ . Several reported efforts in the past on polycrystalline BaM mainly dealt with textured thin and thick films and showed, depending on the degree of texture, an out-of-plane  $H_A$  in the range 4.5 to 15 kOe [31,32]. In this work, however, the BaM component in composites results in overall effective in-plane anisotropy field.

We have also calculated the Gilbert damping coefficient (GDC) [33,34] of the composites by analyzing the FMR spectra of the samples. GDC is a dimensionless quantity which can be used as a measure of the losses in a ferromagnetic material. GDCs of the composites were calculated using the equation,

$$\alpha = \frac{\gamma \Delta H}{4\pi f_r} \quad (2)$$

where  $\alpha$  is the damping coefficient,  $f_r$  is the resonance frequency,  $\Delta H$  is the linewidth that was estimated from the FMR frequency-width for profiles in Figure 5, and  $\gamma$  is the gyromagnetic ratio. Estimated values are given in Table 2. Composites with  $x \leq 47$  show GDC  $\sim 0.024$ , and we get a smaller GDC of less than 0.02 for  $x \geq 60$ , which is indicative of a decrease in the losses in the composites as the NFO increases. The composites seem to have a much larger damping coefficient compared to pure and doped NFO [34,35], but it is smaller than the GDC of BaM [36].

**Table 2.** Fitting parameters for FMR and magnetic parameters for BN<sub>x</sub> composites. Gilbert damping constants are also given.

Sample	FMR Fitting Parameters		Measured Saturation Magnetization, $4\pi M_s$ (kG)	$H_A$ (kOe)	Coercive Field (kOe)	Remanent Magnetization ( $M_r$ ) (kG)	Gilbert Damping Coefficient Calculation	
	$\gamma$ (GHz/kOe)	$4\pi M_{eff}$ (kOe)					Frequency Width (GHz)	Gilbert Damping Coefficient ( $\alpha$ )
BN33	3.17	3.53	2.63	0.90	0.255	0.91	3.071	0.02450
BN38	3.26	3.46	2.68	0.78	0.161	0.77	3.042	0.02452
BN41	3.03	4.80	2.34	2.46	0.124	0.63	3.324	0.02491
BN44	2.96	5.30	2.88	2.42	0.114	0.49	3.35	0.02389
BN47	2.98	5.51	2.88	2.63	0.111	0.59	3.25	0.02354
BN60	2.61	10.07	2.75	7.32	0.089	0.73	2.739	0.01699
BN75	2.71	10.54	2.77	7.77	0.046	1.04	2.943	0.01911
BN85	2.98	7.49	2.92	4.57	0.034	0.73	2.535	0.01635
BN95	2.96	7.25	2.87	4.38	0.035	0.83	2.549	0.01613

### 3.4. Magneto-Electric Effects in the BN<sub>x</sub>-PZT Bilayers

The strength of ME coupling was measured in bilayers of the composites and vendor-supplied PZT (PZT850, American Piezo Ceramics, Mackeyville, PA, USA). Ferrite platelets of approximate lateral dimensions 5 mm × 10 mm and thickness  $t = 0.3$ – $0.5$  mm were bonded to PZT with 20  $\mu$ m thick layer of a fast-dry epoxy. The ME voltage coefficient (MEVC) was measured for two different orientations of the applied magnetic fields: (i)  $\alpha_{31}$  for the DC field  $H$  and ac field  $H_{ac}$  were parallel to each other and along the length of the sample (direction-1), and the induced voltage was measured across the thickness of PZT (direction-3) and (ii)  $\alpha_{33}$  for the magnetic fields was applied perpendicular to the sample plane (direction-3) and induced voltage was measured across PZT thickness. The MEVC is given by  $\alpha = V_3/(H_{ac} t)$ , where  $V_3$  is the strain-induced ac voltage measured across PZT. The ME coefficients were measured at low frequencies, as well as at the mechanical resonances in the bilayers.

Figure 8 (and Figure S6 in the Supplementary Materials) shows the  $H$  dependence of  $\alpha_{31}$  for ac field at 100 Hz. The MEVC is directly proportional to the piezomagnetic coupling  $q = d\lambda/dH$ . The value of  $\alpha_{31}$  increases when  $H$  is increased to the maximum. The maximum value of MEVC for BN5 is rather small due to low  $q$ -value for this BaM rich composite. With further increases in the NFO content in the composites,  $\alpha_{31}$  increases to a maximum value of  $\sim 152$  mV/cm Oe for BN95. Upon further increase in  $H$ ,  $\alpha_{31}$  in general decreases to a minimum for composites with  $x > 5$ . Bias field  $H$  dependence of  $\alpha_{31}$  in Figure 8 essentially tracks the variation in  $q$  with  $H$ , reaches a maximum at the maximum in the slope of  $\lambda_{11}$  vs.  $H$ , and drops to near zero when the magnetostriction (Figure 3) shows near saturation. Other significant features in the results from Figure 8 are as follows. (i) When  $H$  is decreased from  $\sim 3$  kOe back to zero a hysteresis in  $\alpha_{31}$  vs.  $H$  is evident for all the BN<sub>x</sub>-PZT bilayers. (ii) Upon reversing the field  $H$ , a 180 deg phase shift (indicated by negative values for  $\alpha_{31}$ ) is observed in the ME voltage except for  $x = 5$ . (iii) The bilayers show a finite remnant value for  $\alpha_{31}$  at zero-bias that is, as discussed later, attributed to the built-in bias in BN<sub>x</sub> provided by the anisotropy field  $H_A$ .

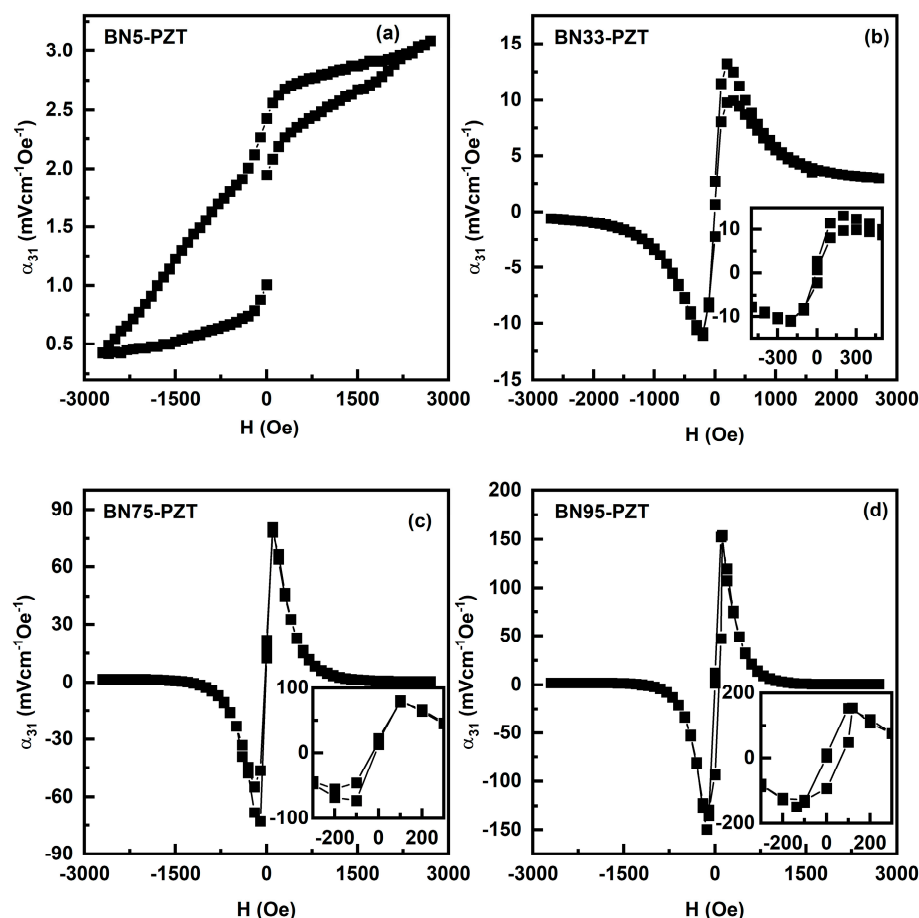


**Figure 8.** Variation of the ME voltage coefficient MEVC  $\alpha_{31}$  with the magnetic field  $H$  for both ac field  $h$  and DC magnetic field  $H$  applied parallel to the ferrite-PZT bilayer for (a) BN5-PZT, (b) BN33-PZT, (c) BN75-PZT and (d) BN95-PZT.

Figure 9 shows results of MEVC measurements for the magnetic fields applied perpendicular to the bilayers of BN $x$ -PZT (also shown in Figure S6). The variation in MEVC has similar hysteresis and remanence as the in-plane magnetic fields. However, the following features in  $\alpha_{33}$  vs.  $H$  differ from the dependence of MEVC for in-plane magnetic fields. (i) Overall MEVC values are smaller in Figure 9 since demagnetization factors reduce both the dc and ac magnetic fields. (ii) The decrease in MEVC for  $H > 1.5$  kOe is relatively small compared to  $\alpha_{31}$  vs.  $H$ . (iii) Data in Figure 9 for BN95-PZT bilayers show a reversal in the sign of for  $H > 0.75$  kOe for both positive and negative  $H$ .

The strength of ME coupling in the bilayers was also characterized by measuring the ac magnetic field frequency  $f$  dependence of the MEVC at mechanical resonance modes. Prior to these measurements, we obtained the electromechanical resonance (EMR) frequencies ( $f_r$ ) for the composites by measuring the frequency dependence of the impedance with an LCR meter. Mode frequencies could not be obtained for BN $x$  for  $x \leq 19$ , but we were able to determine the frequency of longitudinal resonance modes for higher  $x$ -values. MEVC  $\alpha_{31}$  vs  $f$  under a bias field  $H = 100$ – $200$  Oe for the bilayers is shown in Figure 10. One observes an increase in  $\alpha_{31}$  with increasing  $f$  and a sharp peak in its value at  $f_r \sim 55$ – $75$  kHz. We were able to identify  $f_r$  with the longitudinal EMR mode from the known composite dimensions. For  $x = 33$ , the figure shows a fine structure with a double peak in the  $\alpha_{31}$  vs  $f$  profile with values of 147 mV/cm Oe at 72.9 kHz and 132 mV/cm Oe at 73.2 kHz. Bilayers of BN $x$ -PZT with  $x > 33$  have a single peak in the profiles and BN95-PZT shows the highest value of  $\alpha_{31} = 992$  mVcm $^{-1}$ Oe $^{-1}$  at 59 kHz. One observes a significant enhancement in the ME coefficients at  $f_r$  compared to values at 100 Hz (Figure 8), and for example, by a factor 36 for  $x = 41$ . The highest Q-factor obtained from this data is found to be 130.4 for BN44. BN41

also has a large Q-factor of 118. After BN44, the Q-factor reduced to 75 at BN60. We discuss the results of these ME measurements in the following section.

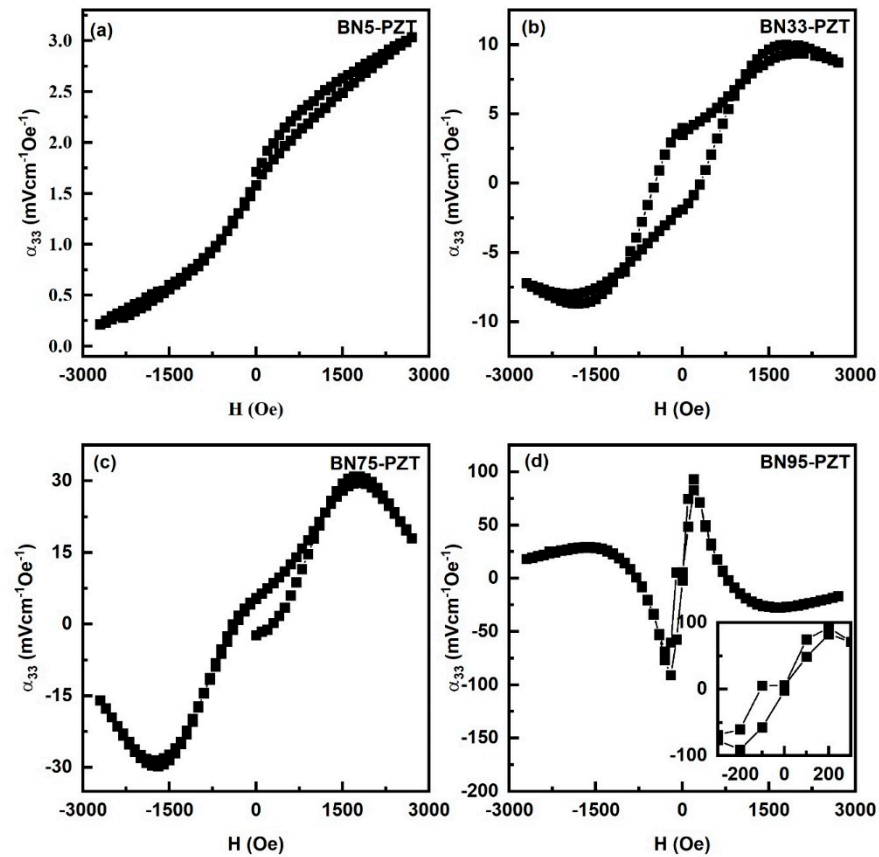


**Figure 9.** Similar MEVC  $\alpha_{33}$  vs. H data as in Figure 7 for H, and h applied perpendicular to the sample plane for bilayers of (a) BN5-PZT, (b) BN33-PZT, (c) BN75-PZT and (d) BN95-PZT.

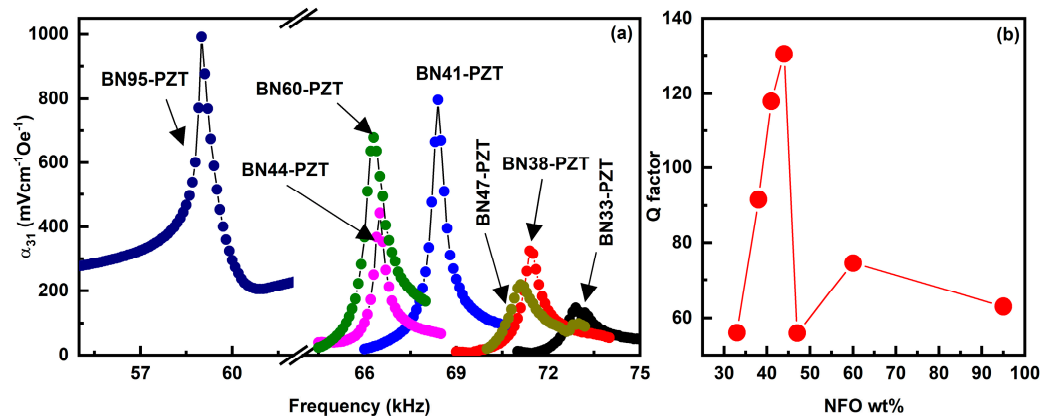


**Figure 10.** (a) Frequency dependence of ME coefficient  $\alpha_{31}$  for bilayer of BN $x$ -PZT. The peak values of MEVC occur at longitudinal mechanical resonance frequency in the samples. (b) Q-factor as a function of NFO weight fraction of BN $x$  composites from the resonance ME response.

#### 4. Discussion

It is evident from the results of this study that (i) it is possible to synthesize composites of spinel and M-type hexagonal ferrites free of ferromagnetic impurity phases, (ii) the composites, depending on the amount of BaM, have a moderately high induced planar anisotropy in all compositions, and (iii) the magnetostriction is quite small for BaM rich composites but increases significantly with increasing NFO content; however, the piezo-

magnetic coefficient  $q$  is rather small in all of the composites due to a slow increase in  $\lambda$  with  $H$  compared to pure NFO.

It is interesting to note that the coercive field estimated from  $M$  vs.  $H$  data for the  $BN_x$  composites remains well under 0.3 kOe for all compositions from  $x = 33$ –95. The coercive field gradually increases from 35 Oe for  $BN_{33}$  to 256 Oe for  $BN_{95}$ .  $BN_{75}$ , the material that has highest anisotropy field of 7.77 kOe, has a coercive field of  $\sim 45$  Oe. It is also important to note that the highest remanent magnetization obtained for  $BN_{75}$  also has the highest anisotropy. The anisotropy acts as a driving force that gives rise to a remanent magnetization for all  $BN_x$  samples and a zero-bias MEVC in bilayers with PZT. All the  $BN_x$  samples remain soft magnetic material with a coercive field less than 300 Oe with no significant hysteresis loss for  $x = 33$ –95. The value of this coercive field is well below the coercive field of pure polycrystalline BaM which possesses a large coercive field  $\sim 5$  kOe. In the composites, the stabilization of the BaM grains (Figure 2) does not seem to increase the coercive field.

It is also clear from the results of ME measurements in Figures 8–10 that the bilayers of  $BN_x$  and PZT show MEVCs that are much higher than the values reported for M-type hexaferrite-PZT bilayers [37], but smaller than those reported for NFO-PZT [38]. Under the optimum value of  $H$ , the highest MEVCs are  $\alpha_{31} = 152$  mV/cm Oe and  $\alpha_{33} = 90$  mV/cm Oe, both for  $BN_{95}$ -PZT. These values, however, are relatively small due to the weak piezomagnetic coupling strengths in  $BN_x$  compared to nickel ferrite or nickel zinc ferrite-based layered composites with PZT [34,39].

A key and primary objective of this work was to synthesize a ferromagnetic oxide with a moderately large  $H_A$  and high magnetostriction and piezomagnetic coupling for use with PZT to achieve ME coupling in the absence of an external bias magnetic field. It is worth noting that this goal was indeed accomplished. Bilayers of  $BN_x$ -PZT used in this study do show a zero-bias MEVC (Figure S7 in the Supplementary Materials). Bilayer of  $BN_{75}$ -PZT shows the highest  $\alpha_{31} = 22$  mV/cm Oe at zero-bias, and the  $BN_{85}$ -PZT bilayer shows the highest  $\alpha_{33} = 9$  mV/cm Oe at zero-bias. It is noteworthy that the remanent magnetization of 1.04 kG for  $BN_{75}$  is the highest for the composites (Table 2). Strategies employed in the past to realize zero-bias ME effects included the use of an external stimuli or functionally graded composites, either in magnetization or in composition, etc. [7–17]. The use of an easy to synthesize composite of a spinel ferrite and hexaferrite in this work for zero-bias ME effect makes this method more viable than others. There are reports wherein composites consisting of NFO and PZT show a large ME coefficient of 460 mV/cm Oe for bilayers and  $\sim 1200$  mV/cm Oe for multilayers [40]. The MEVC at resonance in these systems was as high as  $\sim 1$  V/cm Oe [41]. Modified NFO and PZT multilayers even showed a higher ME coefficient [42]. However, there is hardly any evidence for ME coupling zero-bias effect in these composites [37–43].

Due to very low magnetostriction, BaM is not suitable for strong direct ME coupling, but the very high uniaxial anisotropic field in the system was utilized in this work. Even though BaM grains in our  $BN_x$  composites are expected to be completely randomized, leading to a net zero the anisotropic field, the increase in the NFO content in  $BN_x$  seems to promote the growth BaM grains with in-plane  $c$ -axis and a net in-plane anisotropy field.

Finally, we compared the zero-bias MEVC values with results reported in the past. Use of a nickel zinc ferrite graded either in magnetization or composition in a bilayer with PZT resulted in a zero-bias MEVC of 37 mV/cm Oe. Electric field-induced bending vibration mode generated zero-bias ME effect in lead free system, shows an MEVC  $\sim 30$  mV/cm Oe [9]. The low field hysteresis-based zero-bias effect also showed a value of  $\sim 60$  mV/cm Oe [16]. In our work, we have obtained a zero-bias ME coefficient  $\sim 22$  mV/cm Oe for  $BN_{75}$ -PZT bilayer, which is comparable to the earlier report [10]. The zero-bias ME response in our study could be improved with the use of composites of NFO and M-type strontium ferrite (SrM) or Al substituted SrM or BaM with higher  $\lambda$  than pure BaM. Substituted BaM or SrM may be good choices as they also have anisotropic fields as high as  $\sim 30$  kG [43].

## 5. Conclusions

In this work, we have successfully synthesized a novel ferrimagnetic composite consisting of (i) nickel ferrite with high magnetostriction and (ii) M-type barium hexaferrite with very high magneto-crystalline anisotropy field. The aim was to use such a high- $q$  and high- $H_A$  composite to achieve strong ME coupling in the absence of a bias magnetic field in a bilayer with PZT. BN $x$  composites with  $x = 5$ –95 wt.% had high  $q$  for NFO rich compositions and in-plane  $H_A$  as high as 7.77 kOe for  $x = 75$ . ME voltage coefficient measurements at low frequencies and at resonance modes showed moderately strong ME coupling at zero bias for samples with NFO content  $\geq 33$  wt.%. The highest zero bias MEVC of 21.82 mVcm<sup>-1</sup>Oe<sup>-1</sup> was obtained for BN75-PZT bilayers wherein BN75 also possesses the highest anisotropy. BN41-PZT shows MEVC  $\sim 800$  mVcm<sup>-1</sup>Oe<sup>-1</sup> at electromechanical resonance at 68.4 kHz. The BN $x$ -PZT composites have the potential for use in energy harvesting and sensor technologies.

**Supplementary Materials:** The following supporting information can be downloaded at: <https://www.mdpi.com/article/10.3390/s23249815/s1>. **Figure S1:** X-ray diffraction patterns of BN $x$  composites. All composites bear the signatures of NFO and BaM. We have plotted the stick patterns for NFO (PDF No. 00-003-0875) and BaM (PDF No. 00-007-0276) in the bottom pane to visualize the one-to-one correspondence of the Bragg's' positions of each phase to the respective NFO and BaM lines. **Figure S2:** SEM images of BN $x$  ( $x = 5, 9, 13, 33, 38, 41, 44, 47, 60, 75, 85, \text{ and } 95$ ). Hexagonal BaM grains develop with increasing grain size as the NFO content increases. After BN41, the BaM grains deteriorate in size. SEM images of pure BaM and NFO are also shown at the bottom. **Figure S3:** Magnetization vs. magnetic field data for BN composites. **Figure S4:**  $S_{21}$  vs.  $f$  profiles showing FMR and magneto-dielectric modes in BN $x$  composites at selected bias magnetic fields. **Figure S5:** Ferromagnetic resonance frequency of (a) NFO part and (b) magneto-dielectric mode frequencies of BN $x$  composites are plotted as function of external magnetic field ( $H$ ). **Figure S6:** MEVC at for BN $x$ -PZT bilayers for in-plane magnetic fields (left) and out-of-plane magnetic fields (right). **Figure S7:** Zero bias and maximum achievable ME coefficient for BN $x$ -PZT bilayers in transverse and longitudinal modes.

**Author Contributions:** All authors contributed to this work. Sample synthesis: S.S., S.A. and R.B.; Data curation: S.S., S.A., R.B., T.S., J.P., M.P. and G.S.; formal analysis: S.S. and M.P.; funding acquisition: M.P., M.J., G.S. and M.R.P.; project administration: M.P., M.J., G.S. and M.R.P.; original draft preparation: S.S. and G.S. All authors have read and agreed to the published version of the manuscript.

**Funding:** The research at Oakland University was supported by grants from the National Science Foundation (NSF) (ECCS-1923732, ECCS-EAGER-2236879, DMR-1808892) and the Air Force Office of Scientific Research (AFOSR) Award No. FA9550-20-1-0114. The research at the Taras Shevchenko National University of Kyiv was supported by the Ministry of Education and Science of Ukraine, Project No. 0122U001908. Efforts at the University of Connecticut were supported by the NSF (ECCS-EAGER-2236879). The research at AFRL was partially supported by the AFOSR Award No. FA9550-23RXCOR001.

**Data Availability Statement:** Data are available from the corresponding author upon reasonable request.

**Conflicts of Interest:** The authors declare no conflict of interest.

## References

1. Vopson, M.M. Fundamentals of Multiferroic Materials and Their Possible Applications. *Crit. Rev. Solid State Mater. Sci.* **2015**, *40*, 223–250. [[CrossRef](#)]
2. Fiebig, M.; Lottermoser, T.; Meier, D.; Trassin, M. The evolution of multiferroics. *Nat. Rev. Mater.* **2016**, *1*, 16046. [[CrossRef](#)]
3. Spaldin, N.A.; Ramesh, R. Advances in magnetoelectric multiferroics. *Nat. Mater.* **2019**, *18*, 203–212. [[CrossRef](#)]
4. Nan, C.-W.; Bichurin, M.I.; Dong, S.; Viehland, D.; Srinivasan, G.J. Multiferroic magnetoelectric composites: Historical perspective, status, and future directions. *Appl. Phys.* **2008**, *103*, 031101. [[CrossRef](#)]
5. Eerenstein, W.; Mathur, N.D.; Scott, J.F. Multiferroic and magnetoelectric materials. *Nature* **2006**, *442*, 759–765. [[CrossRef](#)] [[PubMed](#)]
6. Caicedo, J.M.; Zapata, J.A.; Gómez, M.E.; Prieto, P. Magnetoelectric coefficient in BiFeO<sub>3</sub> compounds. *J. Appl. Phys.* **2008**, *103*, 07E306. [[CrossRef](#)]

7. Zhou, Y.; Maurya, D.; Yan, Y.; Srinivasan, G.; Quandt, E.; Priya, S. Self-Biased Magnetolectric Composites: An Overview and Future Perspectives. *Energy Harvest. Syst.* **2016**, *3*, 1–42. [[CrossRef](#)]
8. Liu, S.; Liao, S.; Wei, K.; Deng, L.; Zhao, L.; Zou, H. Self-biased magnetolectric composite for energy harvesting. *Battery Energy* **2023**, *2*, 20230005. [[CrossRef](#)]
9. Yang, S.C.; Cho, K.-H.; Park, C.-S.; Priya, S. Self-biased converse magnetolectric effect. *Appl. Phys. Lett.* **2011**, *99*, 202904. [[CrossRef](#)]
10. Mandal, S.K.; Sreenivasulu, G.; Petrov, V.M.; Srinivasan, G. Flexural deformation in a compositionally stepped ferrite and magnetolectric effects in a composite with piezoelectrics. *Appl. Phys. Lett.* **2010**, *96*, 9916. [[CrossRef](#)]
11. Mandal, S.K.; Sreenivasulu, G.; Petrov, V.M.; Srinivasan, G. Magnetization-graded multiferroic composite and magnetolectric effects at zero bias. *Phys. Rev. B* **2011**, *84*, 014432. [[CrossRef](#)]
12. Sreenivasulu, G.; Mandal, S.K.; Bandekar, S.; Petrov, V.M.; Srinivasan, G. Low-Frequency and Resonance Magnetolectric Effects in Piezoelectric and Functionally Stepped Ferromagnetic Layered Composites. *Phys. Rev. B* **2011**, *84*, 144426. [[CrossRef](#)]
13. Laletin, U.; Sreenivasulu, G.; Petrov, V.M.; Garg, T.; Kulkarni, A.R.; Venkataramani, N.; Srinivasan, G. Hysteresis and remanence in magnetolectric effects in functionally graded magnetostrictive-piezoelectric layered composites. *Phys. Rev. B* **2012**, *85*, 104404. [[CrossRef](#)]
14. Lage, E.; Kirchhof, C.; Hrkac, V.; Kienle, L.; Jahns, R.; Knöchel, R.; Quandt, E.; Meyners, D. Exchange biasing of magnetolectric composites. *Nature Mater.* **2012**, *11*, 523. [[CrossRef](#)] [[PubMed](#)]
15. Borisov, P.; Hochstrat, A.; Chen, X.; Kleemann, W.; Binek, C. Magnetolectric switching of exchange bias. *Phys. Rev. Lett.* **2005**, *94*, 117203. [[CrossRef](#)] [[PubMed](#)]
16. Zhou, Y.; Yang, S.C.; Apo, D.J.; Maurya, D.; Priya, S. Tunable self-biased magnetolectric response in homogenous laminates. *Appl. Phys. Lett.* **2012**, *101*, 232905. [[CrossRef](#)]
17. Yan, Y.; Zhou, Y.; Priya, S. Giant Self-Biased Magnetolectric Coupling in Co-fired Textured Layered Composites. *Appl. Phys. Lett.* **2013**, *102*, 052907. [[CrossRef](#)]
18. Huang, T.; Becerra, L.; Gensbittel, A.; Zheng, Y.; Talleb, H.; Salas, U.A.; Ren, Z.; Marangolo, M. Self-Biased Magnetolectric Ni/LiNbO<sub>3</sub>/Ni Trilayers for Body-Embedded Electronic Energy Harvesters. *Phys. Rev. Appl.* **2023**, *20*, 034059. [[CrossRef](#)]
19. Wu, J.; Du, Y.; Xu, Y.; Qiao, J.; Qu, Y.; Wang, Z.; Dong, S.; Hu, Z.; Liu, M. Self-Biased Magnetolectric Sensor Operating in  $d_{36}$  Face-Shear Mode. *IEEE Sens. J.* **2023**, *23*, 22366. [[CrossRef](#)]
20. Annapureddy, V.; Park, S.H.; Song, H.; Ryu, J. Tunable self-biased magnetolectric effect in magnetization-graded magnetolectric composites. *J. Alloy. Comp.* **2023**, *957*, 170121. [[CrossRef](#)]
21. Aubert, A.; Loyau, V.; Mazaleyrat, F.; LoBu, M. Investigation of Piezomagnetism in Nickel Ferrite. *IEEE Trans. Magn.* **2021**, *57*, 2501105. [[CrossRef](#)]
22. Topal, U. Factors influencing the remanent properties of hard magnetic barium ferrites: Impurity phases and grain sizes. *J. Magn. Magn. Mater.* **2008**, *320*, 331–335. [[CrossRef](#)]
23. Dudziak, S.; Ryżyńska, Z.; Bielan, Z.; Ryl, J.; Klimczuk, T.; Zielińska-Jurek, A. Pseudo-superparamagnetic behaviour of barium hexaferrite particles. *RSC Adv.* **2020**, *10*, 18784. [[CrossRef](#)]
24. An, G.-H.; Hwang, T.-Y.; Kim, J.; Kim, J.B.; Kang, N.; Jeon, K.-W.; Kang, M.; Cho, Y.-H. Novel method for low temperature sintering of barium hexaferrite with magnetic easy-axis alignment. *J. Euro. Ceram. Soc.* **2014**, *34*, 1227–1233. [[CrossRef](#)]
25. Anantharamaiah, P.N.; Prerna Rao, B.; Shashanka, H.M.; Chelvane, J.A.; Khopkar, V.; Sahoo, B. Role of Mg<sup>2+</sup> and In<sup>3+</sup> substitution on magnetic, magnetostrictive and dielectric properties of NiFe<sub>2</sub>O<sub>4</sub> ceramics derived from nanopowders. *Phys. Chem. Chem. Phys.* **2021**, *23*, 1694. [[CrossRef](#)] [[PubMed](#)]
26. Licei, F.; Rinaldi, S. Magnetostriction of some hexagonal ferrites. *J. Appl. Phys.* **1981**, *52*, 2442–2443.
27. Sheen, J. Comparisons of microwave dielectric property measurements by transmission/reflection techniques and resonance techniques. *Meas. Sci. Technol.* **2009**, *20*, 042001. [[CrossRef](#)]
28. Joseph, R.I.; Schlömann, E. Demagnetizing Field in Nonellipsoidal Bodies. *J. Appl. Phys.* **1965**, *36*, 1579. [[CrossRef](#)]
29. Hellwege, K.-H.; Springer, A.M. (Eds.) *Landolt-Bornstein; Numerical Data and Functional Relationships in Science and Technology, Group III, Crystal and Solid State Physics, Volume 4(b), Magnetic and Other Properties of Oxides*; Springer: New York, NY, USA, 1970.
30. Naiden, E.P.; Zhuravlev, V.A.; Minin, R.V.; Itin, V.I.; Korovin, E.Y. Static and dynamic magnetic properties of nanosized barium hexaferrite powders prepared by the sol-gel combustion method. *Russ. Phys. J.* **2015**, *58*, 125. [[CrossRef](#)]
31. Nie, Y.; Harward, I.; Balin, K.; Beaubien, A.; Celinski, Z. Preparation and characterization of barium hexagonal ferrite thin films on a Pt template. *J. Appl. Phys.* **2010**, *107*, 073903. [[CrossRef](#)]
32. Wu, M. M-type barium hexagonal ferrite films. In *Advanced Magnetic Materials*; InTech: Rijeka, Croatia, 2012.
33. Gilbert, T.L. A Phenomenological Theory of Damping in Ferromagnetic Materials. *IEEE Trans. Magn.* **2004**, *40*, 3443. [[CrossRef](#)]
34. Robbenolt, S.; Sasaki, S.S.; Wallace, T.; Bartholomew, M.; Tolbert, S.H. Fabrication and magnetic properties of Sol-Gel derived NiZn ferrite thin films for microwave applications. *Adv. Mater. Lett.* **2018**, *9*, 345. [[CrossRef](#)]
35. Lumetzberger, J.; Buchner, M.; Pile, S.; Ney, V.; Gaderbauer, W.; Daffé, N.; Moro, M.V.; Primetzhofer, D.; Lenz, K.; Ney, A. Influence of structure and cation distribution on magnetic anisotropy and damping in Zn/Al doped nickel ferrites. *Phys. Rev. B* **2020**, *102*, 054402. [[CrossRef](#)]
36. Sharma, V.; Kumari, S.; Kuanr, B.K. Rare earth doped M-type hexaferrites; ferromagnetic resonance and magnetization dynamics. *AIP Adv.* **2018**, *8*, 056232. [[CrossRef](#)]

37. Pan, Q.; Zhang, X.; Xia, B.; Chu, B. Magnetolectric response in laminated BaFe<sub>12</sub>O<sub>19</sub>/Pb(Zr,Ti)O<sub>3</sub> composites. *J. Appl. Phys.* **2023**, *133*, 244101. [[CrossRef](#)]
38. Zhai, J.; Cai, N.; Shi, Z.; Lin, Y.; Nan, C.-W. Coupled magnetodielectric properties of laminated PbZr<sub>0.53</sub>Ti<sub>0.47</sub>O<sub>3</sub>/NiFe<sub>2</sub>O<sub>4</sub> ceramics. *J. Appl. Phys.* **2004**, *95*, 5685–5690. [[CrossRef](#)]
39. Hong-Xia, C.; Qian, S.; Jia-yang, Y.; Yu, F.; Huang, S. Transverse Magnetolectric effect in nickel zinc ferrite/Lead zirconate titanate layered composites. *Adv. Mater. Res.* **2015**, *1061–1062*, 184–188.
40. Srinivasan, G.; Rasmussen, E.T.; Gallegos, J.; Srinivasan, R.; Bokhan, Y.I.; Laletin, V.M. Magnetolectric bilayer and multilayer structures of magnetostrictive and piezoelectric oxides. *Phys. Rev B* **2001**, *64*, 214408. [[CrossRef](#)]
41. Wang, Y.; Yu, Y.; Zeng, M.; Wan, J.G.; Zhang, M.F.; Liu, J.-M.; Nan, C.W. Numerical modeling of the magnetolectric effect in magnetostrictive piezoelectric bilayers. *Appl. Phys. A* **2005**, *81*, 1197. [[CrossRef](#)]
42. Cótica, L.F.; Betal, S.; Morrow, C.T.; Priya, S.; Guo, R.; Bhalla, A.S. Thermal effects in magnetolectric properties of NiFe<sub>2</sub>O<sub>4</sub>/Pb(Zr<sub>0.52</sub>Ti<sub>0.48</sub>)O<sub>3</sub>/NiFe<sub>2</sub>O<sub>4</sub> tri-layered composite. *Integr. Ferroelectr.* **2016**, *176*, 203–209. [[CrossRef](#)]
43. Röschmann, P.; Lemke, M.; Tolksdorf, W.; Welz, F. Anisotropy fields and FMR linewidth in single-crystal Al, Ga and Sc substituted hexagonal ferrites with M structure. *Mater. Res. Bull.* **1984**, *19*, 385. [[CrossRef](#)]

**Disclaimer/Publisher’s Note:** The statements, opinions and data contained in all publications are solely those of the individual author(s) and contributor(s) and not of MDPI and/or the editor(s). MDPI and/or the editor(s) disclaim responsibility for any injury to people or property resulting from any ideas, methods, instructions or products referred to in the content.